

Multi-wavelength VCSEL arrays using high-contrast gratings

Erik Haglund^{*a}, Johan S. Gustavsson^a, Wayne V. Sorin^b, Jörgen Bengtsson^a, David Fattal^c,
Åsa Haglund^a, Michael Tan^b, and Anders Larsson^a

^aPhotonics Laboratory, Department of Microtechnology and Nanoscience,
Chalmers University of Technology, SE-41296, Göteborg, Sweden;

^bHewlett Packard Enterprise, 1501 Page Mill Road, Palo Alto, CA 94304-1123, USA;

^cLEIA Inc., 2440 Sand Hill Road, Menlo Park, CA 94025, USA

ABSTRACT

The use of a high-contrast grating (HCG) as the top mirror in a vertical-cavity surface-emitting laser (VCSEL) allows for setting the resonance wavelength by the grating parameters in a post-epitaxial growth fabrication process. Using this technique, we demonstrate electrically driven multi-wavelength VCSEL arrays at ~980 nm wavelength. The VCSELs are GaAs-based and the suspended GaAs HCGs were fabricated using electron-beam lithography, dry etching and selective removal of an InGaP sacrificial layer. The air-coupled cavity design enabled 4-channel arrays with 5 nm wavelength spacing and sub-mA threshold currents thanks to the high HCG reflectance.

Keywords: high-contrast grating, vertical-cavity surface-emitting laser, wavelength multiplexing, optical interconnect

1. INTRODUCTION

Wavelength division multiplexing (WDM) can be used to improve the capacity and bandwidth density of optical interconnects [1]. As a WDM light source, multi-wavelength VCSEL arrays are attractive as they may offer performance, efficiency, and cost advantages over other technologies. However, monolithic arrays are intrinsically difficult to realize since the resonance wavelength of a conventional VCSEL cavity, defined by the spacing between the two distributed Bragg reflectors (DBRs), is set during epitaxial growth. Replacing the top DBR by a high-contrast grating (HCG) enables the resonance wavelength to be set by the grating parameters in a post-epitaxial growth fabrication process, since the phase of the reflection depends on the grating period and duty cycle [2]. This was previously proposed and analyzed by simulations [3,4], and also demonstrated for optically pumped VCSELs [5].

Using this technique, we have demonstrated electrically driven monolithic multi-wavelength VCSEL arrays at ~980 nm wavelength [6]. The VCSELs are GaAs-based and the suspended GaAs HCGs were fabricated using electron-beam lithography, dry etching and selective removal of an InGaP sacrificial layer. For the resonance wavelength to be sensitive to the phase of the HCG reflection we use an air-coupled cavity design without any additional DBR mirror pairs to boost the reflectivity of the HCG. This requires HCGs with near 100% reflectance. The sub-mA threshold currents and direct reflectivity measurements suggest that the reflectivity of the HCGs is indeed close to 100%. Our air-coupled cavity design has enabled a 4-channel array with 5 nm wavelength spacing.

2. HCG DESIGN, FABRICATION, AND CHARACTERIZATION

HCGs can provide high broadband reflectivity with large polarization and angular dependence [2]. To analyze the properties of our HCGs, which are GaAs-HCGs suspended in air, we use rigorous coupled-wave analysis (RCWA) simulations [7]. Fig.1 compares the spectral reflectance of a GaAs-HCG with 270 nm thickness, 405 nm period, and 60% duty cycle with a regular 21 pair Al_{0.90}Ga_{0.10}As/GaAs DBR, both designed for operation at 980 nm. The graph clearly illustrates the broadband and polarization selecting properties of the HCG. Fig.2 shows the dependence of reflectance and phase of the reflectivity on grating period and duty cycle for the 270 nm thick GaAs-HCG when illuminated with TM-polarized light (electric field perpendicular to the grating bars). Over a range of period/duty cycle combinations, a phase variation >60° can be achieved while maintaining a reflectance > 99.8% at a wavelength of 980 nm.

*erik.haglund@chalmers.se; phone: +46-739-086224

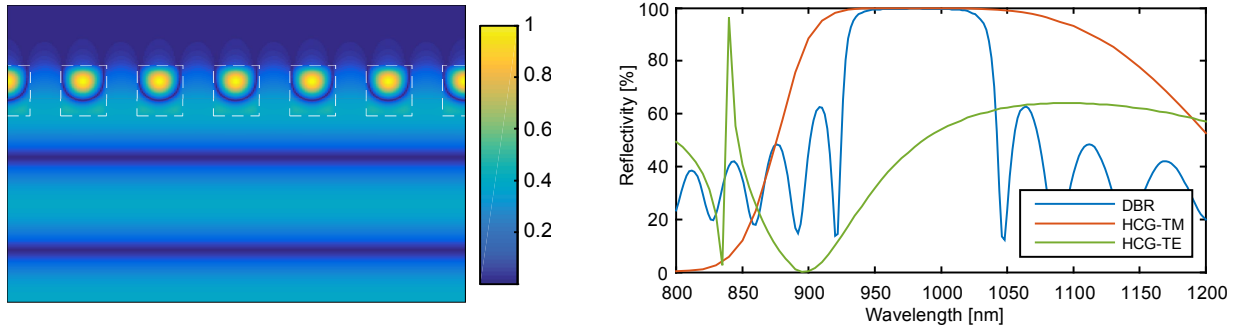


Figure 1. Normalized electrical field strength of a TM plane wave incident on a HCG simulated by RCWA (left) and spectral reflectance (right) for the suspended GaAs-HCG with thickness = 270 nm, period = 405 nm, and duty cycle = 60% under TM (red) and TE (green) illumination. Comparison to a 21 pair $\text{Al}_{0.90}\text{Ga}_{0.10}\text{As}/\text{GaAs}$ DBR (blue) is also included.

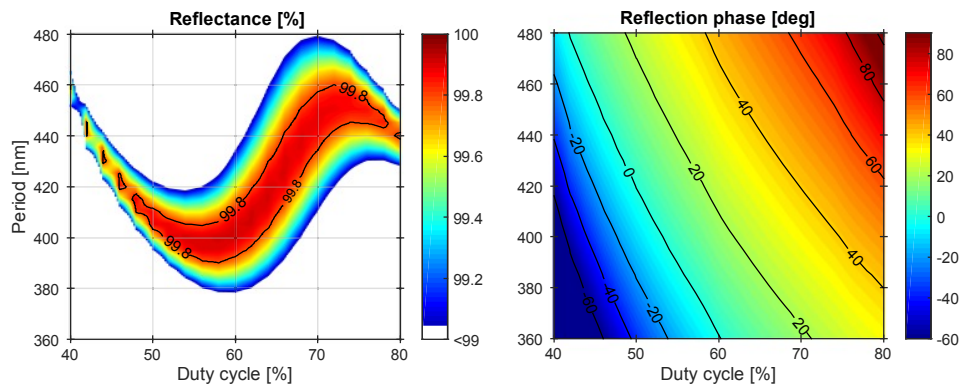


Figure 2. Reflectance (left) and phase of reflection (right) for a suspended GaAs-HCG as a function of period and duty cycle under TM illumination at 980 nm. The HCG thickness is 270 nm.

In our design, the 270 nm GaAs-HCG layer is p -doped at $5 \cdot 10^{18} \text{ cm}^{-3}$ to enable current injection outside the HCG area. The high field strength in the grating bars (Fig.1) gives rise to large free-carrier (hole) absorption. This was accounted for in the simulations presented in Figs.1 and 2 by assuming a free-hole absorption coefficient of [8]:

$$\alpha(\text{cm}^{-1}) = 7 \cdot 10^{-18} \cdot N_A(\text{cm}^{-3}) \quad (1)$$

where N_A is the acceptor concentration. Fig.3 shows the dependence of reflectance, transmittance, and loss on hole concentration for the GaAs-HCG. Clearly, the presence of free holes reduces the reflectance and increases the amount of

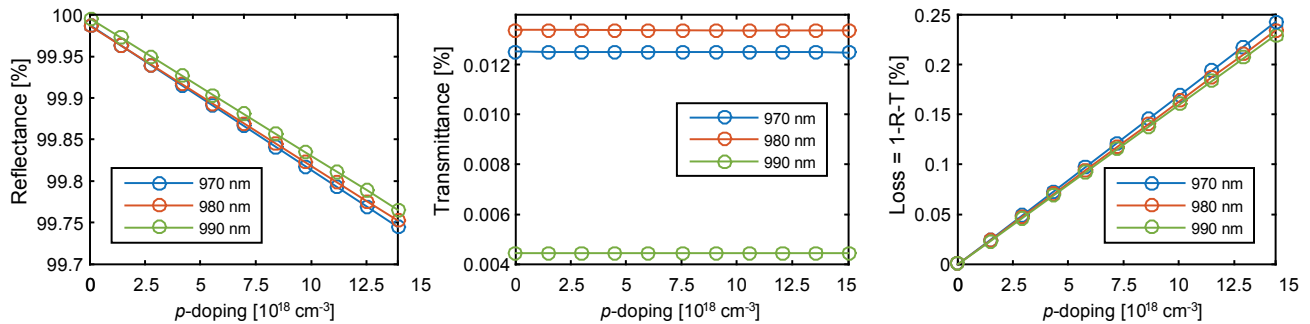


Figure 3. Dependence of reflectance (left), transmittance (middle), and loss (right) on hole concentration for a suspended GaAs-HCG under TM illumination at 970, 980, and 990 nm. HCG thickness = 270 nm, period = 405 nm, and duty cycle = 60%.

light absorbed in the HCG. Interestingly, the transmittance is unaffected by absorption and therefore the reduction in reflectance is due to an increase of loss. With significantly more of the non-reflected light being absorbed than transmitted, an HCG-VCSEL with a *p*-doped HCG used as the outcoupling mirror is expected to suffer from reduced slope efficiency.

The fabrication process for the suspended HCG is illustrated in Fig.4. It starts with definition of an etch mask in ZEP520A resist by electron beam lithography, followed by etching into an underlying lattice-matched $\text{In}_{0.49}\text{Ga}_{0.51}\text{P}$ sacrificial layer by highly anisotropic SiCl_4 reactive ion etching. The sacrificial InGaP layer was then removed using concentrated HCl with high selectivity against GaAs [9]. Finally, the liquid was removed using critical point drying to avoid stiction. The SEM images of a fabricated HCG in Fig.5 show that the grating bars are straight with smooth surfaces and have a rectangular cross-section. When etching InGaP in HCl , the etch rate is highly dependent on the crystal orientation with preferential etching in the $\langle 100 \rangle$ directions and no etching in the $\langle 110 \rangle$ directions [9]. The grating bars were therefore oriented along $\langle 100 \rangle$, as illustrated in Fig.5.

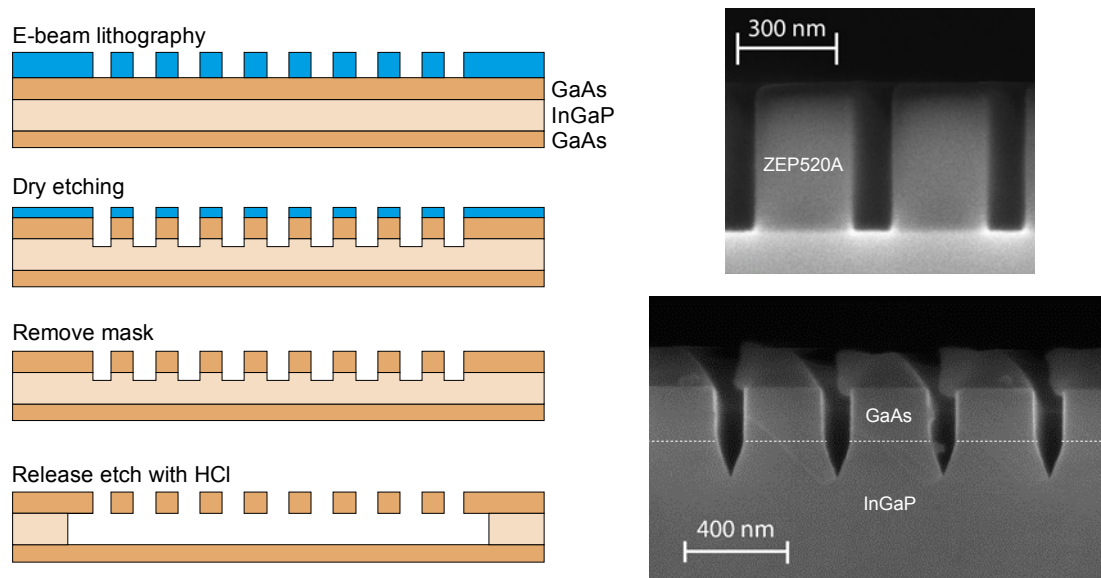


Figure 4. Left: The HCG fabrication process. Right: SEM images after ZEP520A electron beam resist exposure and development (upper) and after dry etching through the GaAs-HCG layer and into the InGaP sacrificial layer (lower).

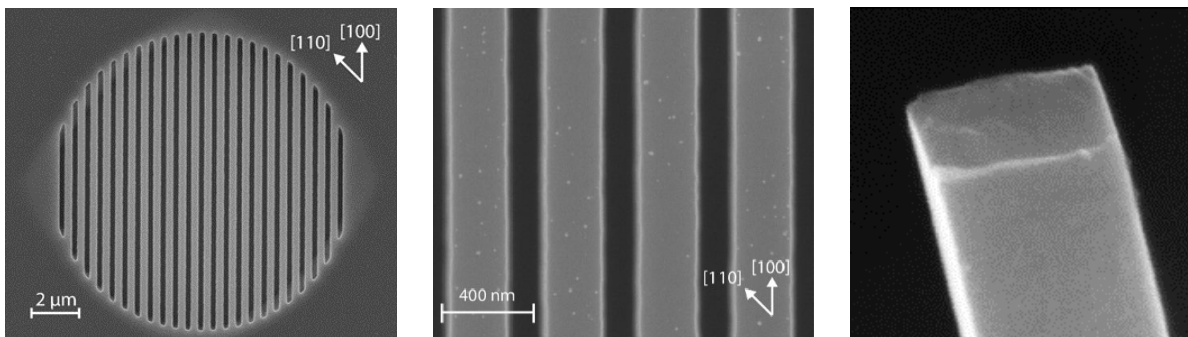


Figure 5. SEM images of suspended GaAs-HCG. Left: the full HCG. Middle: close-up showing the smoothness of the grating bars. Right: cross-sectional view of a broken grating bar.

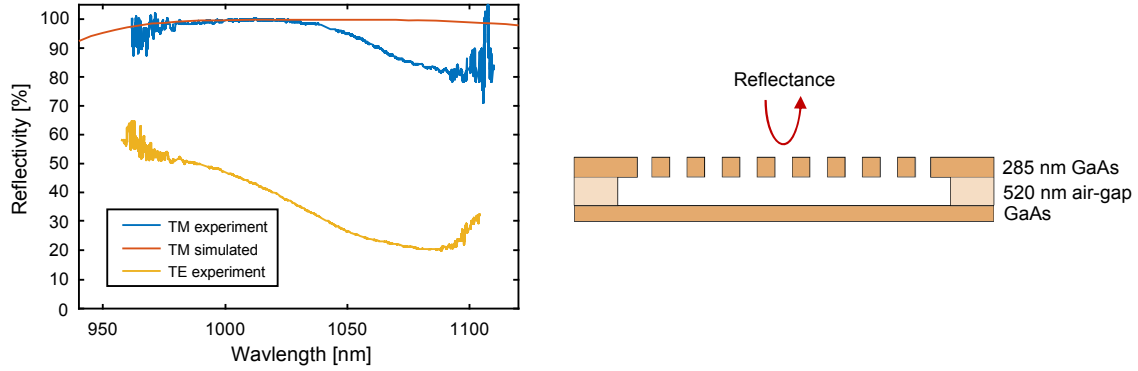


Figure 6. Measured and simulated spectral reflectance for a test GaAs-HCG with thickness = 285 nm, period = 435 nm, and duty cycle = 63%. The simulation accounts for the 520 nm air-gap under the HCG and the GaAs below the air-gap.

The measured spectral reflectance (using a fiber-coupled superluminescent diode and a lens-package to focus the incident light on the HCG and collect the reflected light) and its polarization dependence for a fabricated GaAs-HCG of thickness 285 nm, period 435 nm, and duty cycle 63% is shown in Fig.6, where it is also compared to the simulated reflectance under TM illumination. The measured reflectance was calibrated against the reflectance from an Au layer deposited next to the HCG, assuming a wavelength independent Au reflectance of 98% [10]. The measurements confirm the high reflectance at ~1010 nm wavelength and the strong polarization dependence predicted by the simulations.

3. HCG-VCSEL DESIGN, FABRICATION, AND CHARACTERIZATION

The design of the surface emitting HCG-VCSEL with a suspended GaAs-HCG as the top mirror is illustrated in Fig.7. The epitaxial structure, grown by MOCVD on an *n*-doped GaAs substrate, contains an *n*-doped 37 pair $\text{Al}_{0.90}\text{Ga}_{0.10}\text{As}/\text{GaAs}$ DBR, an active region with partly strain compensated InGaAs/GaAsP quantum wells (QWs), a $3\lambda/4$ thick *p*-doped GaAs current spreading layer, a *p*-doped InGaP sacrificial layer with an equivalent air thickness of $\lambda/2$, and a 270 nm thick *p*-doped GaAs HCG layer. A 30 nm thick $\text{Al}_{0.98}\text{Ga}_{0.02}\text{As}$ layer was placed both below and above the active region for the formation of oxide apertures for transverse current and optical confinement. The design is intended for lasing at ~980 nm wavelength.

The resonance wavelength of the VCSEL cavity is set by the round-trip phase condition:

$$\Phi_{rt} = \Phi_{top} + 2 \cdot \Phi_{cav} + \Phi_{bottom} = m \cdot 2\pi \quad (2)$$

where Φ_{top} and Φ_{bottom} are the reflection phase of the top and bottom mirrors, respectively, Φ_{cav} is the phase accumulated by traversing the cavity separating the mirrors, and m is an integer. The resonance wavelength of the HCG-VCSEL cavity can therefore be set by the grating parameters since the HCG reflection phase (Φ_{top}) is strongly dependent on grating period and duty cycle (Fig.2).

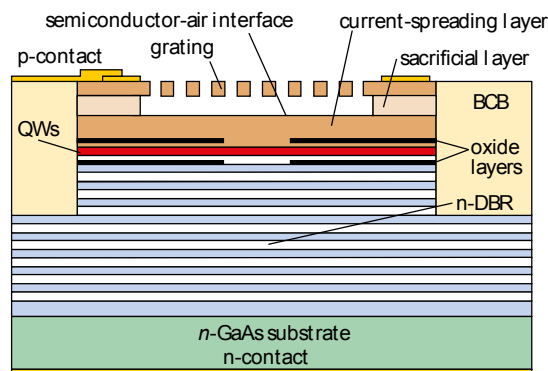


Figure 7. Cross-sectional view of the HCG-VCSEL design.

For large tunability by the grating parameters, the resonance wavelength should be highly sensitive to the HCG reflection phase. This prohibits the use of a few DBR pairs under the HCG to boost the reflectance of the top mirror [11], since it would limit the tunability to only ~ 2 nm. It also requires that the semiconductor-air interface of the current spreading layer is positioned at a node of the standing-wave longitudinal optical field (referred to as an air-coupled cavity design) as opposed to positioning the interface at an anti-node of the field (referred to as a semiconductor-coupled cavity design) [12]. The two different cavity designs are illustrated in Fig.8.

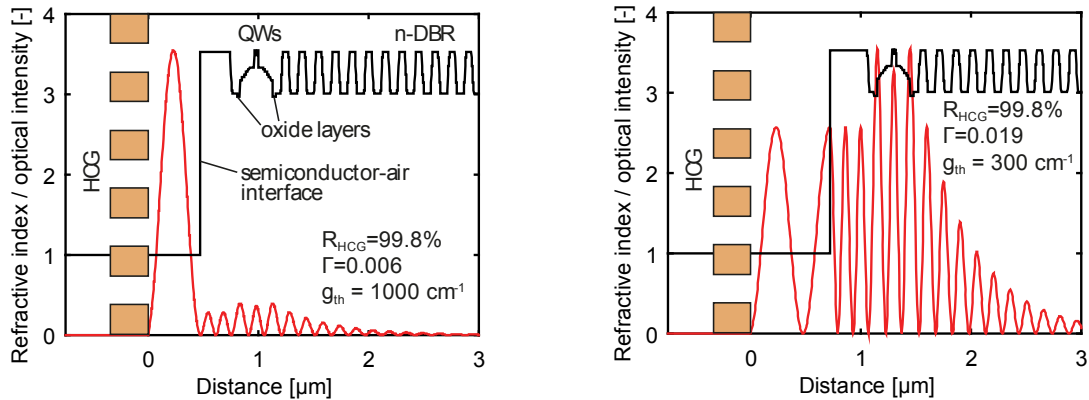


Figure 8. Illustrations of air-coupled (left) and semiconductor-coupled (right) cavity designs. The calculations assume an HCG reflectance of 99.8%.

To analyze the optical cavity properties, we use a 1D transfer-matrix model with input data on HCG reflection obtained from RCWA simulations. Fig.8 shows that in the air-coupled cavity design the longitudinal optical field is strongly confined to the air-gap. As a consequence, the longitudinal optical field confinement to the QWs is low (0.6%), giving a relatively high threshold gain (1000 cm^{-1}). For the semiconductor-coupled cavity design, the longitudinal optical field is more confined to the QWs (1.9%), yielding a lower threshold gain (300 cm^{-1}). However, the tunability is 5-10 times less than for the air-coupled cavity design.

The dependence of threshold gain and resonance wavelength on HCG period and duty cycle for our air-coupled cavity design is shown in Fig.9. A wide wavelength span of 40 nm can be obtained with threshold gain $< 1000 \text{ cm}^{-1}$ using HCGs with period in the range 400-450 nm and duty cycle in the range 45-75%.

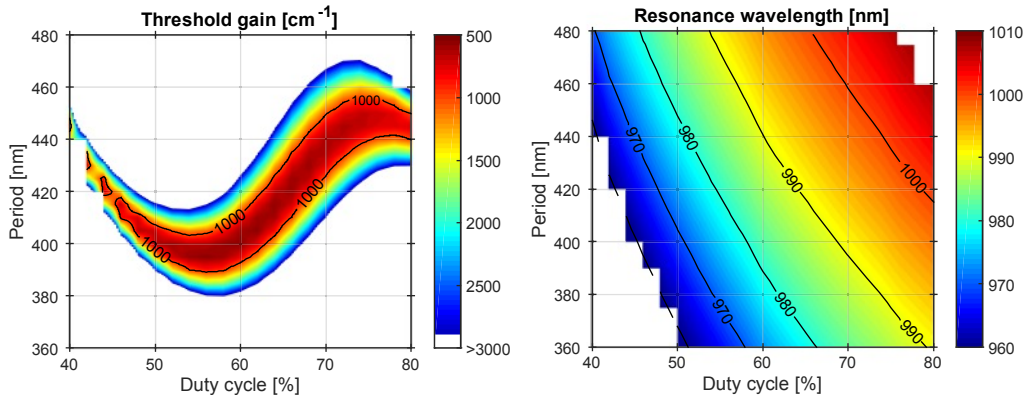


Figure 9. Dependence of threshold gain (left) and resonance wavelength (right) on grating parameters for the air-coupled HCG-VCSEL cavity design.

The VCSELs were fabricated using standard techniques for the fabrication of oxide confined VCSELs, involving contact metal deposition, mesa etching, and selective oxidation. A layer of BCB was used to planarize the structure (Fig.7). As a final step, the suspended HCG was fabricated using the process described in Section 2.

Fig. 10 shows the output power vs. current and spectral characteristics of HCG-VCSELs with oxide aperture diameters of 5, 7, and 15 μm and corresponding HCG diameters of 12, 14, and 22 μm . The relatively low threshold currents (0.5, 0.8, and 2.0 mA), together with the low longitudinal optical confinement factor of the air-coupled cavity design, suggests that the reflectance of the HCG is very high, even higher than that of a regular top DBR. Single-mode emission with a higher order mode suppression of >40 dB was observed for oxide aperture diameters up to 7 μm due to the strong angular dependence of the HCG reflectance.

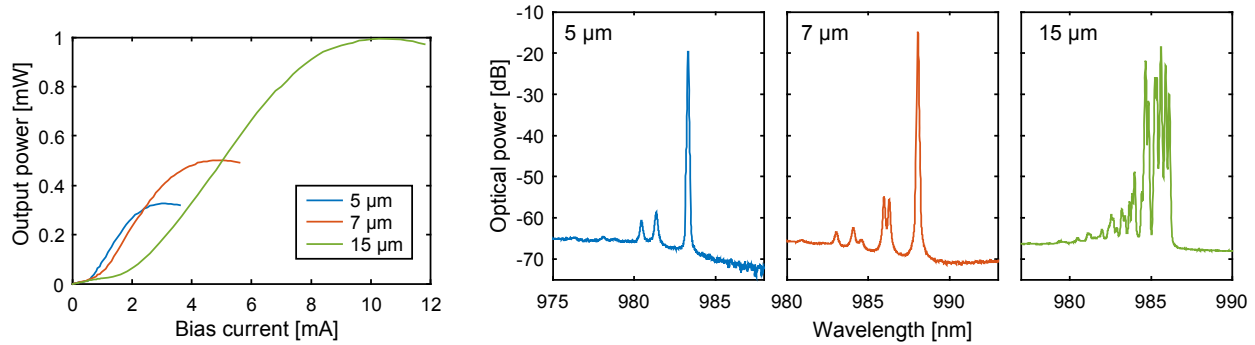


Figure 10. Output power vs. current (left) and emission spectra (right) for HCG-VCSELs with 5, 7, and 15 μm oxide aperture diameters. Spectra are measured at 3, 4, and 9 mA, respectively.

An array of four VCSELs, all having a 5 μm oxide aperture but different combinations of HCG period and duty cycle to set the emission wavelengths individually, was also fabricated and the results are shown in Fig. 11. With the grating period/duty cycle combinations stated in the figure caption, emission wavelengths with 5 nm spacing centered around 985 nm were obtained. The measured wavelengths are in very good agreement with those predicted by our simulations with the specific grating parameters used in the array. The higher order mode suppression is >30 dB at all four emission wavelengths. This is the first demonstration of an electrically driven monolithic multi-wavelength VCSEL array with the emission wavelengths set by the grating parameters of the HCGs used as top mirrors.

All our HCG-VCSELs have relatively low slope efficiency and output power. This is most likely caused by the free-carrier absorption in the p -doped GaAs-HCG (as discussed in Section 2), and maybe also to some extent by a too high HCG reflectivity.

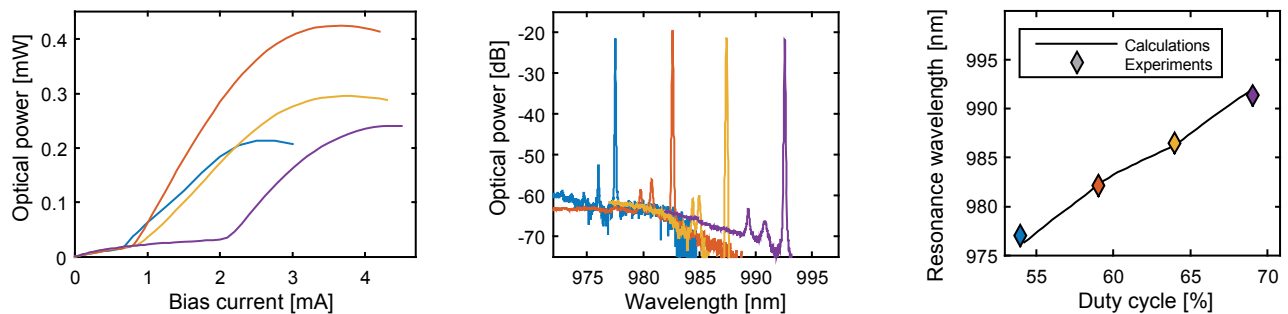


Figure 11. Output power vs. current (left), emission spectra (middle) for an array of HCG-VCSELs with 5 μm oxide aperture diameter, and resonance wavelength vs. duty cycle (right). HCG period/duty cycle: 405 nm/54% (blue), 405 nm/59% (red), 400 nm/64% (yellow), and 410 nm/69% (purple). Spectra are measured at 2, 2, 2, and 3 mA, respectively.

4. SUMMARY AND DISCUSSION

The dependence of the HCG reflection phase on the grating parameters was used to demonstrate, for the first time, post-epitaxial growth wavelength setting of electrically driven HCG-VCSELs. An air-coupled cavity configuration was used to increase the sensitivity of the resonance wavelength to a variation of the reflection phase, thus enabling a large

wavelength setting span. In spite of the low optical field confinement to the QWs for this cavity configuration, lasing with low threshold currents was demonstrated, indicating very high HCG reflectances. A 4-channel monolithic multi-wavelength VCSEL arrays with a wavelength spacing of 5 nm was demonstrated. Thus, lasing was observed over a wavelength span of 15 nm, which is in excellent agreement with our numerical predictions. In addition, this is the first report on suspended GaAs-HCGs using an InGaP sacrificial layer, which may be etched with high selectivity against GaAs.

We expect an improvement of the uniformity of threshold current over the array with a more optimal set of grating parameters such that the variation of threshold gain compensates the spectral variation of gain in the QWs. We also expect an improvement of slope efficiency and output power by the use of an undoped GaAs-HCG layer. This requires etching down to the *p*-doped InGaP sacrificial layer or the *p*-GaAs current spreading layer before top-contact metal deposition.

5. ACKNOWLEDGEMENT

This work was supported by Hewlett Packard Enterprise (HPE), the Swedish Foundation for Strategic Research (SSF), and the Swedish Research Council (VR). The epitaxial material was provided by IQE Europe. Professor Mattias Hammar at the Royal Institute of Technology is acknowledged for providing epitaxial material for test structures.

REFERENCES

- [1] R. Motaghianezam et al., "Four 45 Gbps PAM4 VCSEL based transmission through 300 m wideband OM4 fiber over SWDM4 wavelength grid," *Opt. Exp.* 24(15), 17193 (2016).
- [2] C.J. Chang-Hasnain et al., "High-contrast gratings for integrated optoelectronics," *Adv. Opt. Photon.* 4, 379 (2012).
- [3] J.H.E. Kim et al., "DBR, sub-wavelength grating, and photonic crystal slab Fabry-Perot cavity design using phase analysis by FDTD," *Opt. Exp.* 15(16), 10330 (2007).
- [4] V. Karagodsky et al., "Monolithically integrated multi-wavelength VCSEL arrays using high-contrast gratings," *Opt. Exp.* 18(2), 694 (2010).
- [5] C. Sciancalepore et al., "III-V-on-Si photonic crystal vertical-cavity surface-emitting laser arrays for wavelength division multiplexing," *IEEE Photon. Technol. Lett.* 24(12), 1111 (2013).
- [6] E. Haglund et al., "Demonstration of post-growth wavelength setting of VCSELs using high-contrast gratings," *Opt. Exp.* 24(3), 1999 (2016).
- [7] <http://www-personal.umich.edu/~zlei/>
- [8] H.C. Casey et al., *Heterostructure Lasers*, Academic Press (1978).
- [9] M. J. Cich et al., "Crystallographic dependence of the lateral undercut wet etching rate of InGaP in HCl," *Appl. Phys. Lett.* 82(4), 651 (2003).
- [10] J.M. Bennett et al., "Infrared reflectance and emittance of silver and gold evaporated in ultrahigh vacuum," *Appl. Opt.* 4(2), 221 (1965).
- [11] C. Chang-Hasnain et al., "High-Contrast Grating VCSELs," *IEEE J. Sel. Top. Quantum Electron.* 15(3), 869 (2009).
- [12] F. Sugihwo et al., "Micromachined widely tunable vertical cavity laser diodes," *J. Microelectromech. Syst.* 7(1), 48 (1998).